Available online at www.sciencedirect.com

SciVerse ScienceDirect

Ceramics International 38 (2012) 2793–2802

CERAMICS INTERNATIONAL

www.elsevier.com/locate/ceramint

Interfacial characterization of silicon nitride/silicon nitride joints brazed using Cu-base active metal interlayers

M. Singh [a], J. Martinez Fernandez [b,*], R. Asthana [c], J. Ramirez Rico [b]

[a] Ohio Aerospace Institute, NASA Glenn Research Center, Cleveland, OH 44135, USA

[b] Dpto. Física de la Materia Condensada-ICMSE, Universidad de Sevilla-CSIC, Avda. Reina Mercedes, s/n, 41012 Sevilla, Spain

[c] Department of Engineering & Technology, University of Wisconsin-Stout, Menomonie, WI 54751, USA

Received 16 October 2011; accepted 18 November 2011

Available online 28 November 2011

Abstract

Silicon nitride/silicon nitride joints were vacuum brazed at 1317 K for 5 min and 30 min using ductile Cu-base active metal interlayers. The joints were characterized using scanning electron microscopy (SEM), energy dispersive spectroscopy (EDS), electron back scattered diffraction (EBSD), and transmission electron microscopy (TEM). An inhomogeneous Ti-rich reaction layer (~2–3 μm thick) formed in 5 min at the Si_3N_4/braze interface. The inhomogeneity disappeared after brazing for 30 min and was replaced with a compact and featureless reaction zone. TEM studies revealed fine grains in the reaction layer, and larger grains in the inner part of the joint interfaces. The joints were crack-free and presented features associated with plastic deformation, which indicated accommodation of strain associated with CTE mismatch. Electron Backscatter diffraction (EBSD) revealed a highly textured braze alloy interlayer and its crystallographic orientation was determined. The formation of additional phases at the joint interface during brazing is discussed.

Keywords: A. Joining; B. Electron microscopy; B. Interfaces; D. Si_3N_4; Active metal interlayer

1. Introduction

Silicon nitride ceramics possess excellent high-temperature strength and creep resistance. They are projected to significantly raise engine efficiency and performance when used as turbine components in the next-generation turbo-shaft engines without the extensive cooling that is needed for metallic parts. In the last few decades, considerable amount of research has been done on joining of silicon nitride to itself and to metals. One key aspect of Si_3N_4 utilization in such applications is its response to joining via brazing which is the most widely used method to join ceramics [1–5].

As with brazing of most ceramics, promoting wetting through reactions at the interface between Si_3N_4 and braze improves the adhesion. A wide variety of braze compositions containing active metals have been evaluated including Ni–Cr, Fe–Cr, Ni–Cr–Si, Ni–Cr–B, Au–Pd–Ti, Pd–Ni–Ti and Cu–Pt–Ti/Nb alloys. Besides chromium and titanium as active metals, vanadium (e.g., in Ni–Au–V fillers) has been used to braze Si_3N_4 ceramics and Pd/CuTi interlayers have been used for partial liquid phase bonding.

Among the active metal interlayers (braze filler metals) that have been used to join Si_3N_4 ceramics [2,6–10], Ag–Cu eutectic alloys containing Ti have been most widely used. Contact angle measurements [11,12] reveal that Ti-containing Cu and Ag-base brazes rapidly wet Si_3N_4 ceramics, and the most significant gains are achieved at small (2–10%) amounts of Ti at which braze ductility is not impaired but there is sufficient Ti activity for reaction and bond formation with Si_3N_4. Besides Ti, active elements such as Hf, Zr, Nb and Ta also have been used in braze alloys to join Si_3N_4 to itself and to metals [13–16].

The Ag–Cu–Ti fillers ($T_L < 1200$ K) are known to produce the highest levels of joint integrity in Si_3N_4 ceramics and are some of the most widely used brazes to join Si_3N_4. However, these alloys have relatively low temperature (<800 K) capability, and low thermal and oxidation resistances [9]. There is thus considerable interest in evaluating higher

* Corresponding author.
E-mail address: martinez@us.es (J. Martinez Fernandez).

0272-8842/$36.00
doi:10.1016/j.ceramint.2011.11.050

temperature brazes with better oxidation resistance. In this study, an active braze alloy based on Cu–Al–Si–Ti system, Cu-ABA, with liquidus temperature ($T_L \sim 1297$ K) and oxidation resistance superior to Ag–Cu–Ti brazes was used to join Si_3N_4. In an earlier work [17], we had compared the oxidation kinetics of Cu-ABA with two other Ti-active brazes, Ticusil and Ticuni, using thermo-gravimetric analysis (TGA) at 1023–1123 K. We had found that Cu-ABA had the smallest weight gain and most sluggish oxidation kinetics; it exhibited a marginal saturation weight gain (<0.05 mg cm^{-2}) in 200 min. Cu-ABA has large Cu content (92.8%) which protects it against oxidation (the Pilling–Bedworth ratios of Cu_2O and CuO are <2). The alloying elements Si and Al in Cu-ABA also form protective scales; the PB ratios of Si and Al are 2.27 and 1.28, respectively (Si is known to exhibit an anomalous behavior in that even though its PB ratio >2, it forms a protective oxide scale). Thus, Si_3N_4 joints made using Cu-ABA are expected to provide higher use temperatures and better oxidation resistance than the widely used Ag–Cu–Ti brazes. The Si_3N_4/Si_3N_4 joints made using Cu-ABA were examined for microstructure and composition using scanning electron microscopy (SEM), energy dispersive X-ray spectroscopy (EDS), electron backscattered diffraction (EBSD) and transmission electron microscopy (TEM).

2. Materials and methods

Kyocera Si_3N_4 (SN-281) was used in the joining work. The material contains about 9–10 wt% Lu_2O_3 and has an acicular, interlocking grain structure and fine distribution of intergranular amorphous phases [18]. A commercial Cu–Si–Al–Ti braze alloy, Cu-ABA, with a nominal composition of 92.75Cu–3Si–2Al–2.25Ti, and the solidus and liquidus temperatures of $T_S \sim 1231$ K and $T_L \sim 1297$ K, respectively, was obtained as a foil (thickness $\sim$50 μm) from Morgan Advanced Ceramics, Hayward, CA. The Cu-ABA braze is ductile (42% elongation) and the elastic modulus, yield strength and tensile strength of the braze are 96 GPa, 278 MPa, and 520 MPa, respectively, and its coefficient of thermal expansion (CTE) is 19.5×10^{-6}/K.

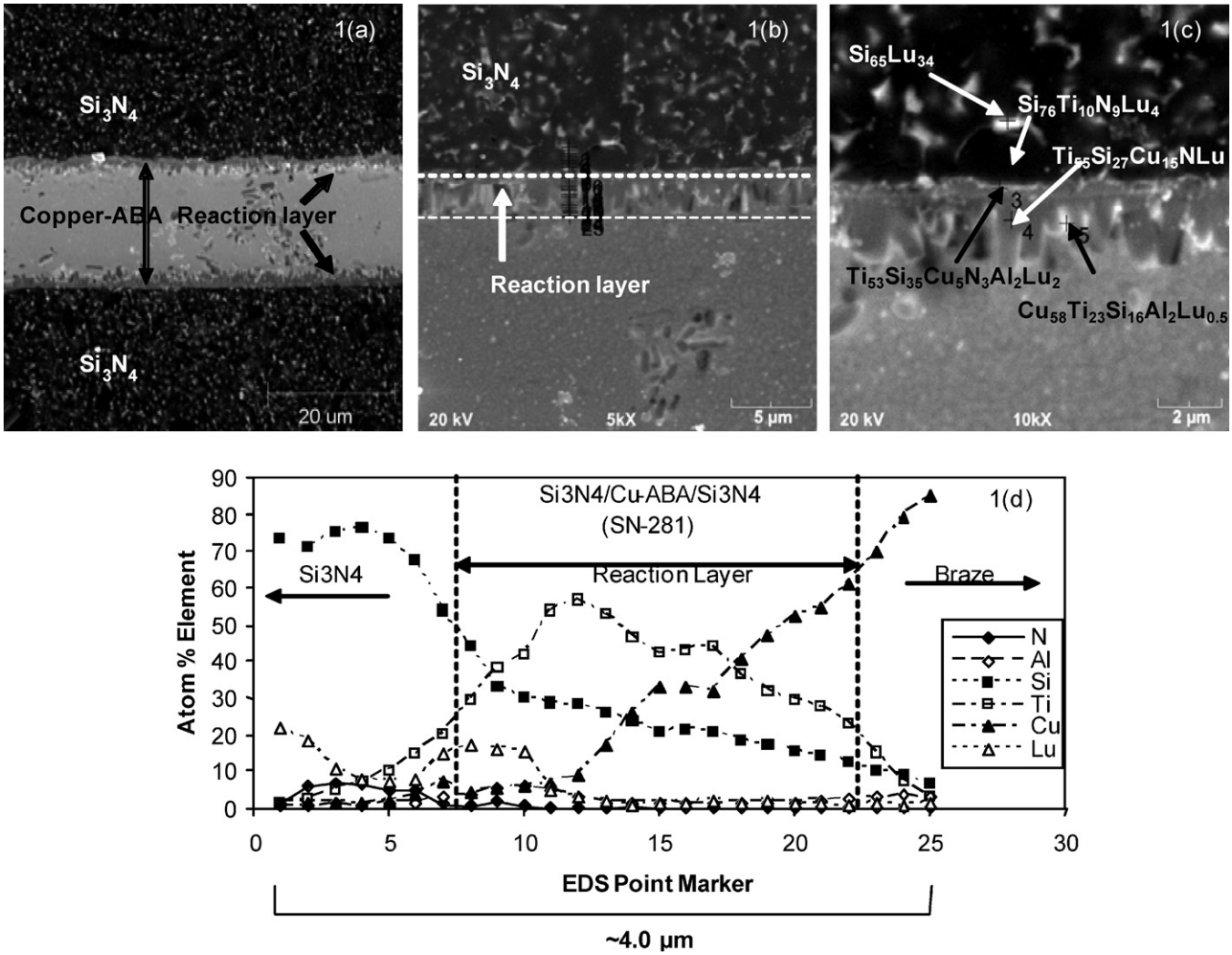

Fig. 1. (a)–(c) Joint microstructure and (d) elemental distribution in self-joined Kyocera SN-281 Si_3N_4 material brazed at 1317 K for 5 min. The EDS data in (d) correspond to the point markers shown in (b).

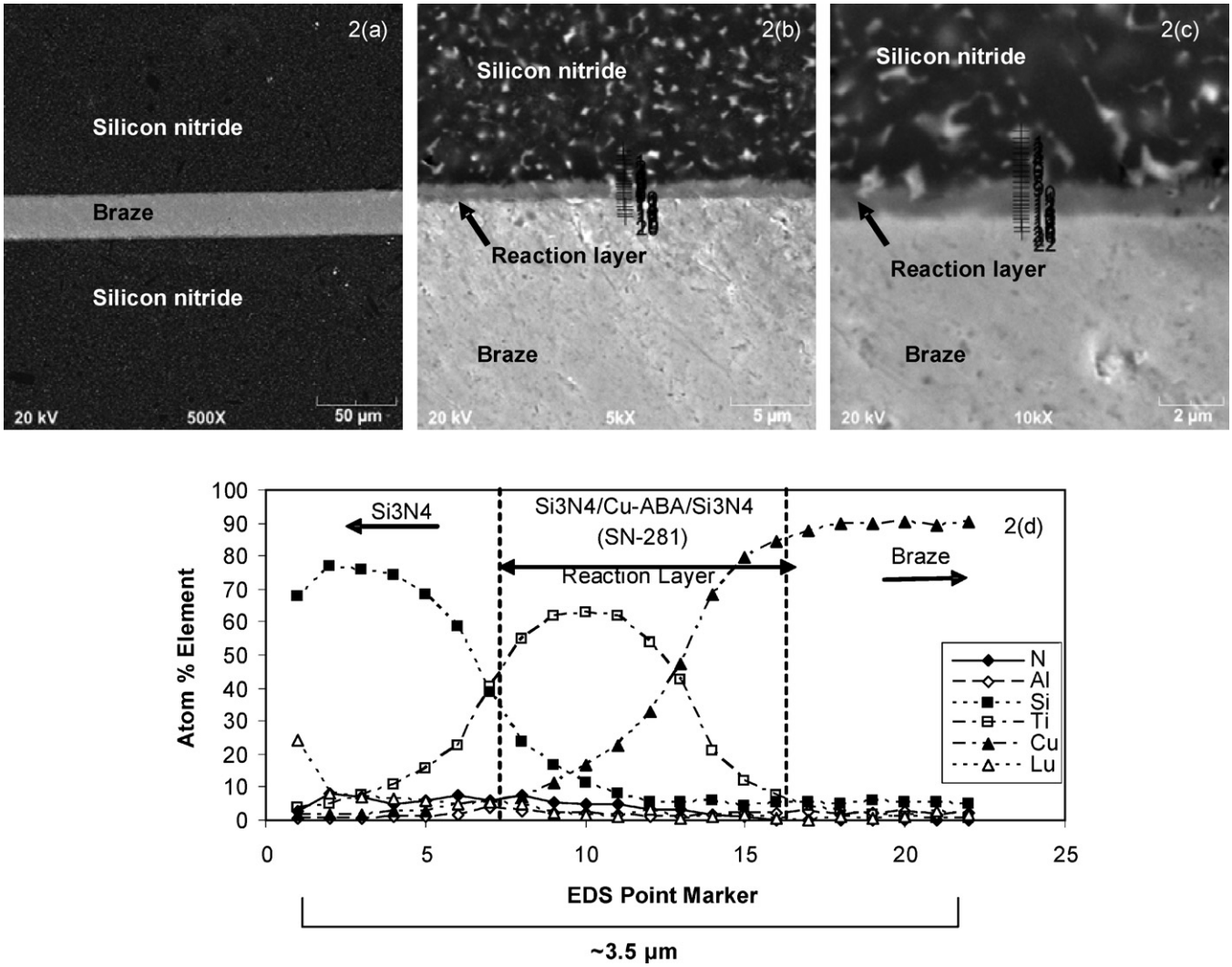

Fig. 2. (a)–(c) Joint microstructure and (d) elemental distribution in self-joined Kyocera SN-281 Si_3N_4 material brazed at 1317 K for 30 min. The EDS data in (d) correspond to the point markers shown in (c).

The substrates and braze foils were sliced into 2.54 cm × 1.25 cm × 0.25 cm pieces, and ultrasonically cleaned in acetone for 15 min. Two braze foils were sandwiched between the substrates, and a load of ∼1–2 N (∼3.5–7.2 kPa pressure) was applied during brazing. The assembly was heated in a furnace to ∼15–20 K above braze liquidus temperature under vacuum ($\sim 10^{-6}$ torr), soaked for either 5 min or 30 min, and slowly cooled to room temperature.

The brazed joints were prepared for metallurgical examination and observed using scanning electron microscopy on a Philips XL30[1], JEOL 840[2], and Hitachi S-5200[1] electron microscopes. Energy dispersive X-ray spectroscopy was also performed on the joints and compositional maps were obtained. Foils were prepared from slices cut perpendicular to the joints using conventional techniques and ion thinned to electron transparency. Transmission electron microscopy observations were done using a Philips CM200 electron microscope[1].

For electron backscattered diffraction measurements, an additional ion milling step was performed as described previously [19]. No conductive coating was applied to the samples. Electron energy was 25 keV, and the samples were tilted at 70° with respect to beam direction. The observations were carried out using a TSL Digiview camera in a Philips XL-30 SEM[1]. The data analysis was performed using TSL OIM Analysis v3.5 software.

The EBSD technique has been described elsewhere [20–26]. In brief, the electron beam of an SEM is diffracted by the sample surface when tilted adequately. The resulting diffraction pattern, a Kikuchi pattern, can be recorded using a digital camera and indexed by a computer program to calculate the orientation of the sample volume that is interacting with the beam. By using the scanning capabilities of an SEM, thousands of equidistant points on the sample surface can be measured automatically, generating orientation maps in which crystallographic data is spatially resolved.

[1] CITIUS, University of Seville, Spain.
[2] NASA Glenn Research Center, USA.

Indexed diffraction patterns with a confidence index lower than 0.2 were discarded.

3. Results and discussion

The joint microstructures and the corresponding EDS analyses are shown in Figs. 1 and 2. Fig. 1 shows a Si_3N_4/Cu-ABA/Si_3N_4 joint made with a brazing time of 5 min at 1317 K. A reaction layer, about 2–3 μm thick, developed at the Si_3N_4/Cu-ABA interface (Fig. 1b and c); this layer has an inhomogeneous structure and morphology. Fig. 1c shows the average composition (in atom %) at different areas (points 1–5). The relative atomic percentages of the major alloying elements (N, Al, Si, Ti, Cu and Lu) over a 4.0 μm distance across the interface are shown in Fig. 1(d). The reaction layer is comprised of a dark-gray, Ti–Si rich phase, possibly titanium silicide, and a lighter Cu-rich phase that also contains Si and Ti (point 5, Fig. 1c). The formation of titanium silicide compounds is thermodynamically favored at the brazing temperature as discussed later.

The crystals of the product phase in the reaction layer of Fig. 1(c) are oriented perpendicular to the interface which presumably is the direction of crystal growth. The distribution of Lutetium from the sintering aid Lu_2O_3 in the Kyocera SN-281 material is also shown in Fig. 1(d). There is no interfacial excess of Lu; it exists in minute quantities in the reaction layer and its concentration progressively increases toward the silicon nitride substrate.

Fig. 2(a)–(c) shows a Si_3N_4/Cu-ABA/Si_3N_4 joint made with 30 min brazing time. The elemental profiles for this joint are shown in Fig. 2(d). An increase of brazing time from 5 min to 30 min did not increase the reaction layer thickness; however, morphologically a more homogeneous, compact, and featureless reaction layer developed in 30 min (Fig. 2c). This featureless product phase presumably formed from the coalescence of coarsened silicide crystals. The absence of an increase in the reaction layer thickness upon increasing the brazing time from 5 min to 30 min indicates fast reaction kinetics in the early stages when the product phase growth is controlled by the rate of the chemical reaction. Later, when an appreciable thickness has developed, the growth kinetics is limited by the slower process of diffusion of reacting species across an already formed reaction layer.

Si_3N_4 material brazed at 1317 K for 30 min was studied in depth as this is presumed to be the stable microstructure in service. EDS compositional maps were obtained in the SEM (Fig. 3) to determine the elemental spatial distribution. The compositional maps showed clearly that titanium was mainly deposited at the Cu-ABA/Si_3N_4 interface. Only small clusters containing Ti remain in the joint interior, whereas the copper was uniformly distributed along the joint region. It is interesting to note how the Ti-rich clusters are spatially coincident with Si-rich areas and copper-depleted areas. Fig. 4(a) shows a higher magnification compositional map focused on the Cu-ABA/Si_3N_4 interface that gives further detail of the elemental distribution in that area. The composition obtained by

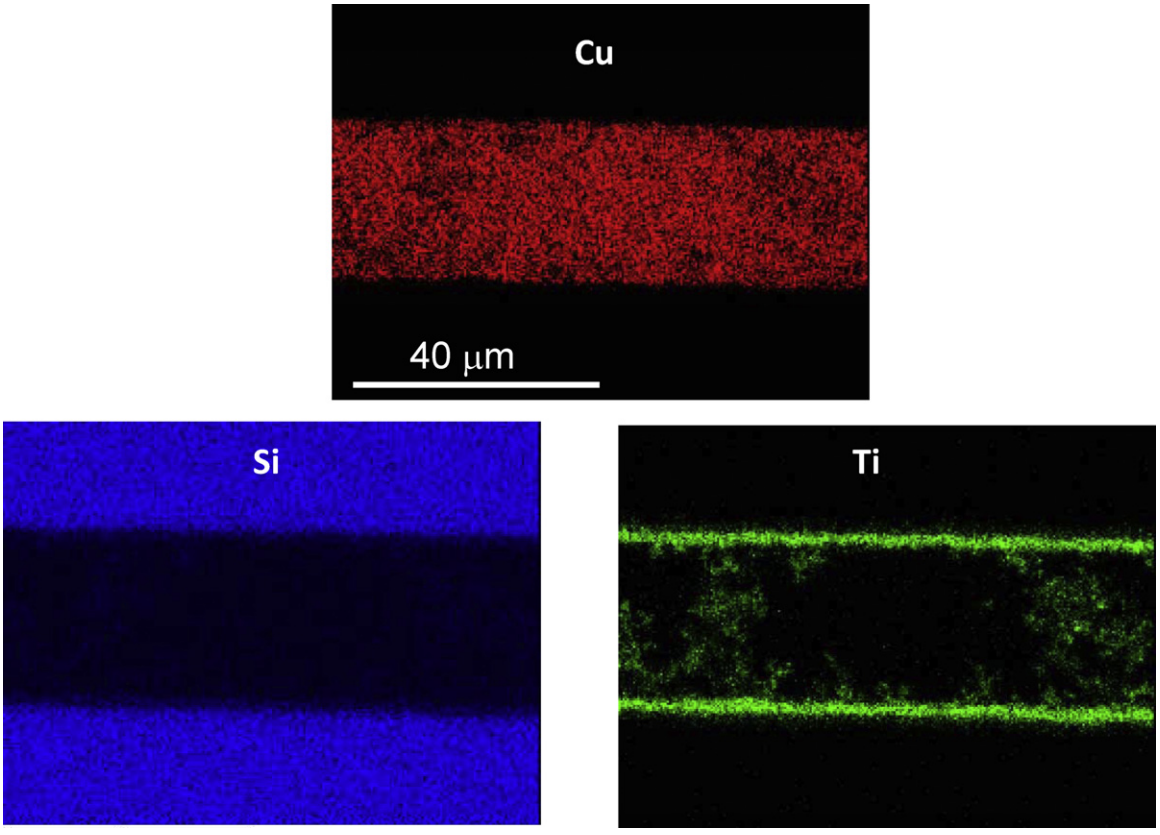

Fig. 3. Cu, Si, and Ti EDS compositional maps of a joint fabricated with 30 min brazing time. Titanium segregation to the reaction layer can be easily visualized.

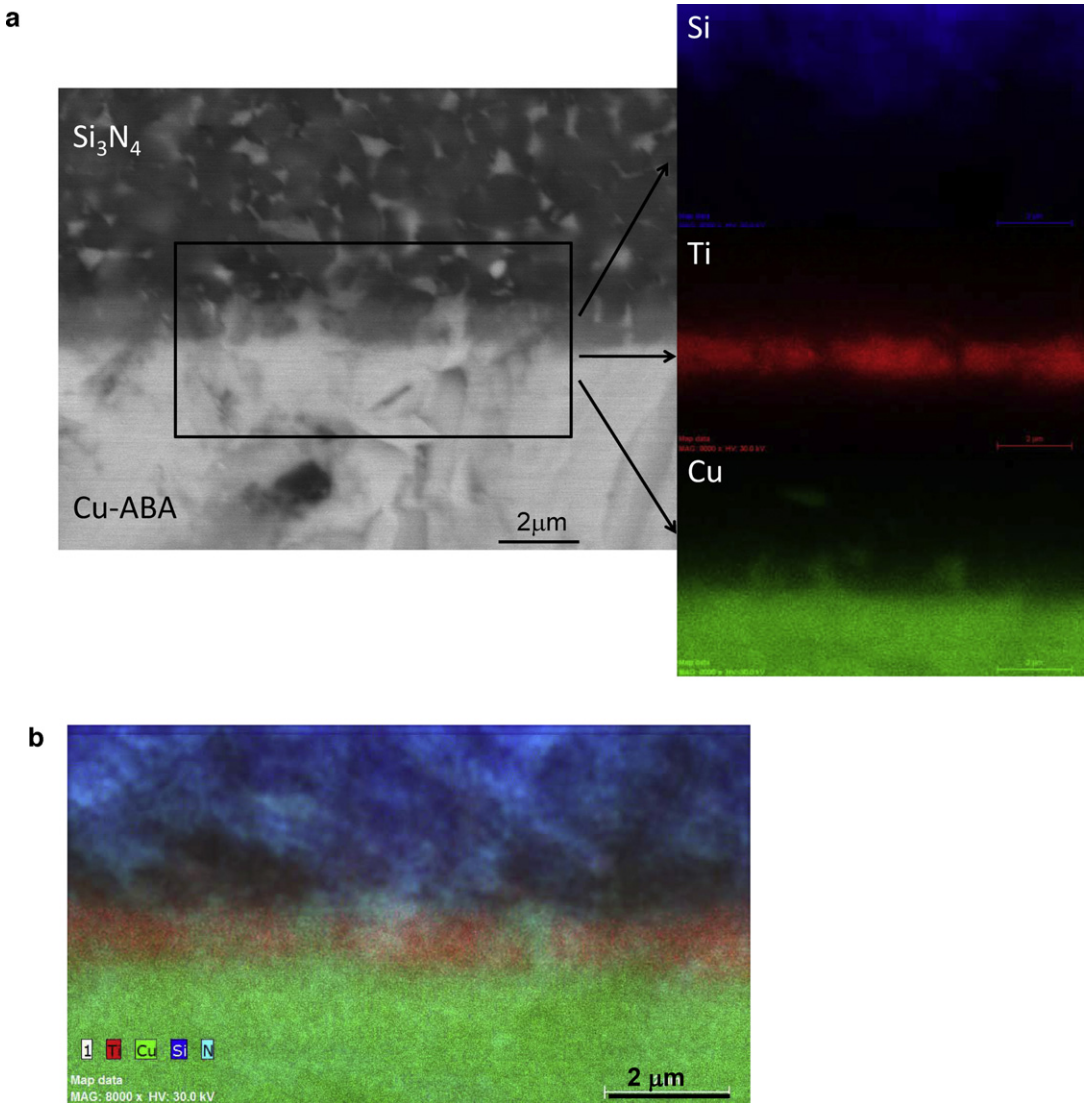

Fig. 4. (a) Higher magnification EDS compositional map focus on the Cu-ABA/Si_3N_4 interface that gives further detail of the elemental distribution on that area. (b) Composition obtained by superimposing the EDS compositional maps of the joint.

superimposing the EDS compositional maps of the joint (Fig. 4b) shows clearly the complementarity of the Ti-rich and Cu-rich areas. The EDS compositional line scan obtained by SEM (Fig. 5) agrees with the previous observations and quantification and gives additional spatial resolution. The high Ti concentration at the Cu-ABA/Si_3N_4 interface is clear. The composition scan obtained by superimposing the line EDS profiles (Fig. 5) shows very clearly the relative position of the compositional distributions.

Clear EBSD patterns could be acquired for Cu-ABA in the joint. No significant charging was observed. Fig. 6 shows an orientation map superimposed to diffraction pattern quality, showing preferred orientation of the Cu-ABA grains. It is interesting to note how the grain orientation is uniform along the joint as indicated by the purple and green bands in Fig. 6. However, there is a rotation of the grains across the joint, perpendicularly to the joint plane. This rotation from approximately a (1 1 0) orientation to a (1 1 2) orientation is indicated by an arrow on the pole figure of Fig. 6. Dark bands inside the joint are probably due to plastic deformation that originated during brazing; this indicates the ability of the brazing layer to accommodate the residual stresses by plastic deformation. The reaction layer and Si_3N_4 could not be observed under EBSD due to polishing/*Z*-number differences between the different layers in the joint.

Pole figures calculated from EBSD data were acquired from an area that covered the width of the joint. Fig. 7(a) presents the (0 0 1), (0 1 1), and (1 1 1) pole figures calculated from EBSD orientation data for Cu. The texture is of ‘‘cube’’ type, characteristic of recrystallized metal under pressure, with the (1 1 1) pole approximately normal to the joint plane. The inverse pole figure calculated from EBSD orientation data of Cu-ABA shown in Fig. 7(b) confirms the highly textured characteristic of the brazing alloy.

TEM observations (Fig. 8) showed that the Si_3N_4 phase and the Cu-ABA region of the joint had a morphology consisting of

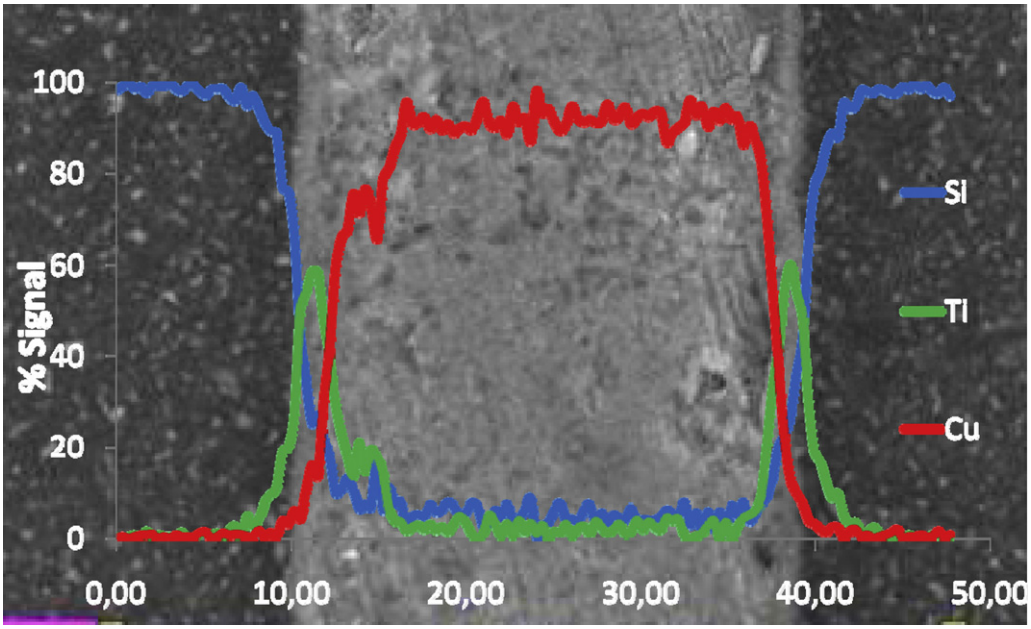

Fig. 5. Composition obtained by superimposing the line EDS profiles that shows the relative position of the compositional distributions.

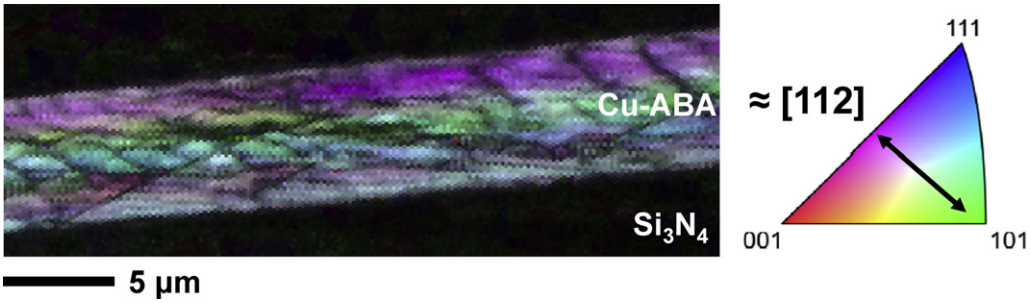

Fig. 6. EBSD orientation map superimposed to diffraction pattern quality, showing preferred orientation of the Cu grains.

large grains (micron size), but the reaction layer microstructure had finer grains (in the range of 20–50 nm). The interfaces between these three regions did not show cracks associated with the brazing process. It is interesting to note that the reaction layer thinned during ion milling at a much slower rate than the metallic inner part of the joint and the Si_3N_4, indicating the formation of new phases.

Fig. 8 includes together with the TEM micrographs showing details of the reaction layer/Si_3N_4 interface, and inner braze regions, insets of their corresponding diffraction patterns. It must be noted that it was very challenging to obtain diffraction patterns of the reaction layer/Si_3N_4 interface, due to the higher thickness of the foil in this region. Special thinning techniques were required. The Cu-ABA layer has the same face centered cubic structure of pure copper. The large Cu grains in Fig. 8 have the (1 1 0) plane perpendicular to the joint plane (the TEM foils were prepared perpendicular to the joint plane), and the (1 1 1) plane approximately parallel to the joint plane. This orientation agrees with the orientation determined by EBSD as the cubic grains could rotate from (1 1 0) to (1 1 2) maintaining the (1 1 1) plane parallel to the joint plane. The rings formed by the spots on the diffraction patterns taken at the reaction layer are an indicative of the small size and relatively random orientation of the grains. Its analysis indicates that the crystallographic structure is face-centered cubic with a lattice parameter of 4.2 ± 0.1 Å, which is in very good agreement with the TiN structure (Fm-3m, $a = 4.239$ Å) [27], but rules out the crystallographic structures of Ti_5Si_3 ($P6_3/mcm$, $a = 7.429$ Å, $c = 5.139$ Å) [27], $TiSi_2$ (Fddd, $a = 8.267$ Å, $b = 4.800$ Å, $c = 8.550$ Å) [27], and AlN ($P6_3mc$, $a = 3.111$ Å, $c = 4.992$ Å) [28]. The presence of other phases in the reaction zone in addition to TiN, however, cannot be ruled out with this analysis as the ion thinning of the reaction area was very slow compared to the surrounding areas, which resulted in a small electron transparent region. In addition, different phases within the reaction zone could have different thinning rates. The formation of TiN and Ti_5Si_3 has also been reported by Loehman et al. [3] in Norton's NC132 Si_3N_4 (which contained MgO) in contact with Cusil-ABA and Ticusil, by Suganuma et al. [1] in bonding of Ti and Si_3N_4, by Naka et al. [29] in Si_3N_4 brazing using an amorphous $Cu_{50}Ti_{50}$ filler

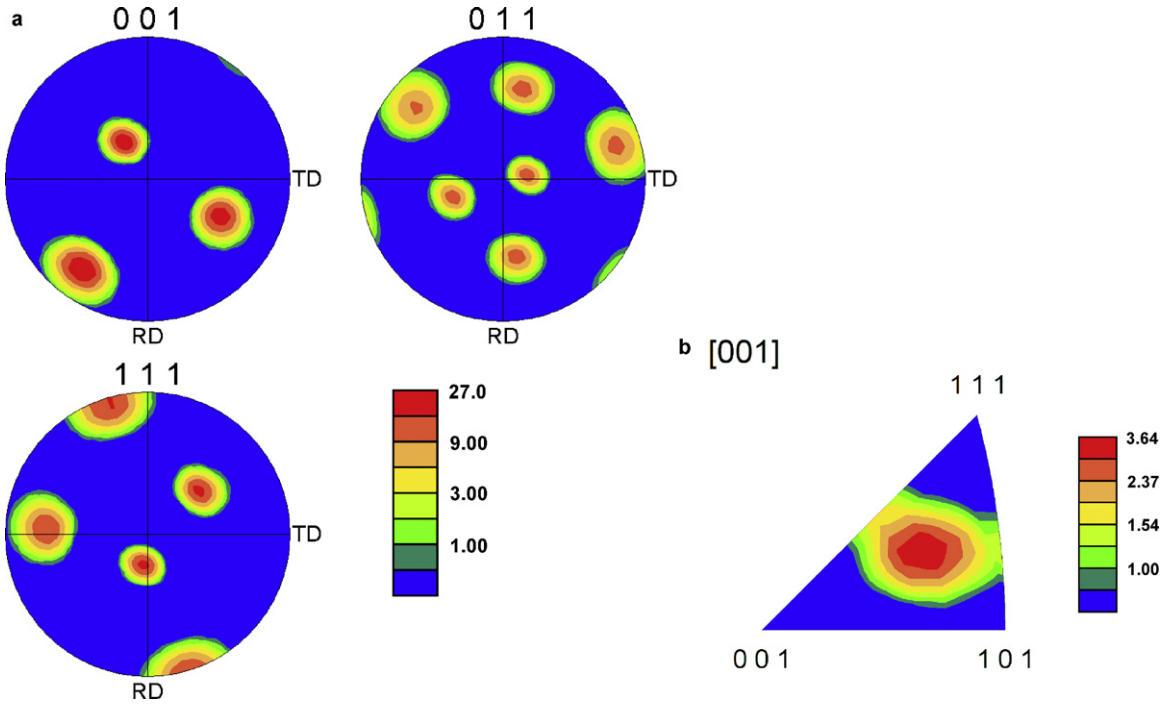

Fig. 7. (a) Pole figures on the [1 0 0], [1 1 0], and [1 1 1] axes calculated from EBSD orientation data for Cu and (b) inverse pole figure calculated from EBSD orientation data of Cu showing the highly textured characteristic of the brazing alloy.

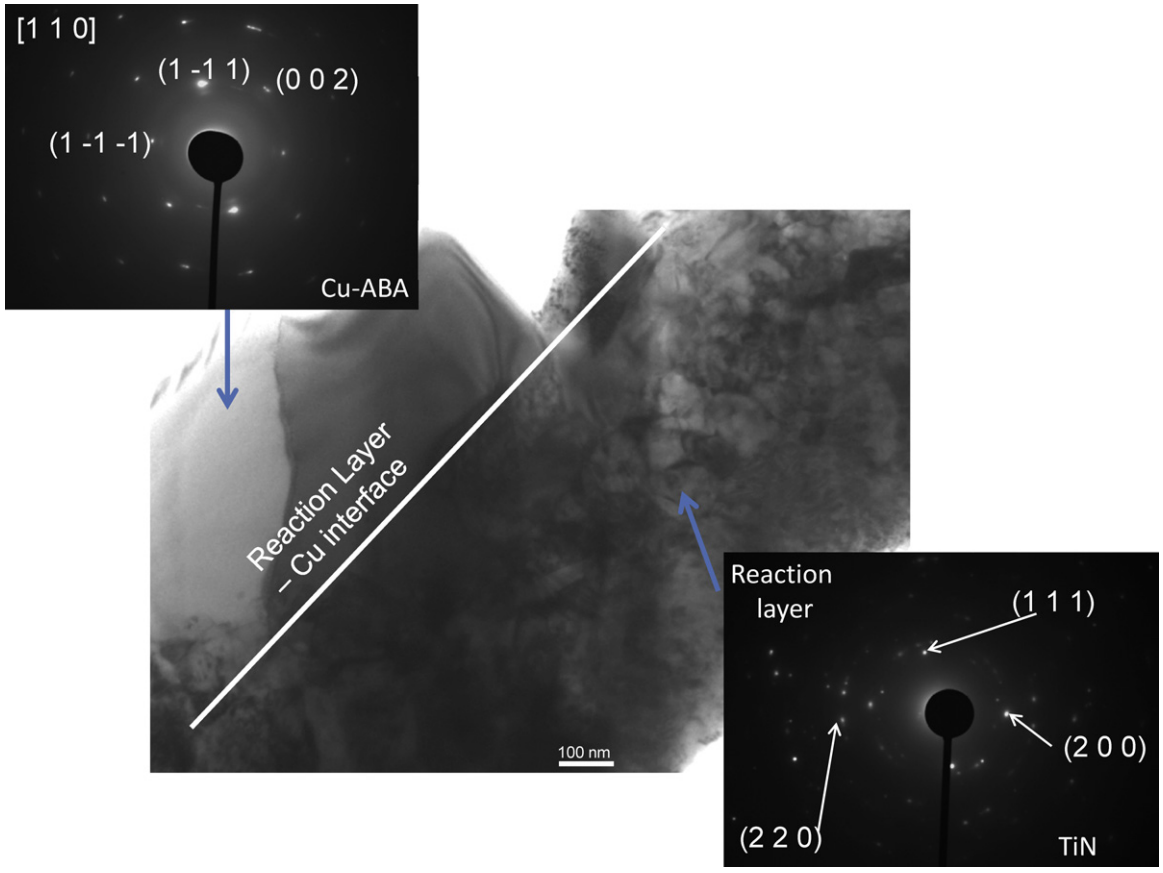

Fig. 8. TEM micrograph showing the microstructure of the reaction layer and adjacent Cu grains. Electron diffraction patterns of these two regions are also included.

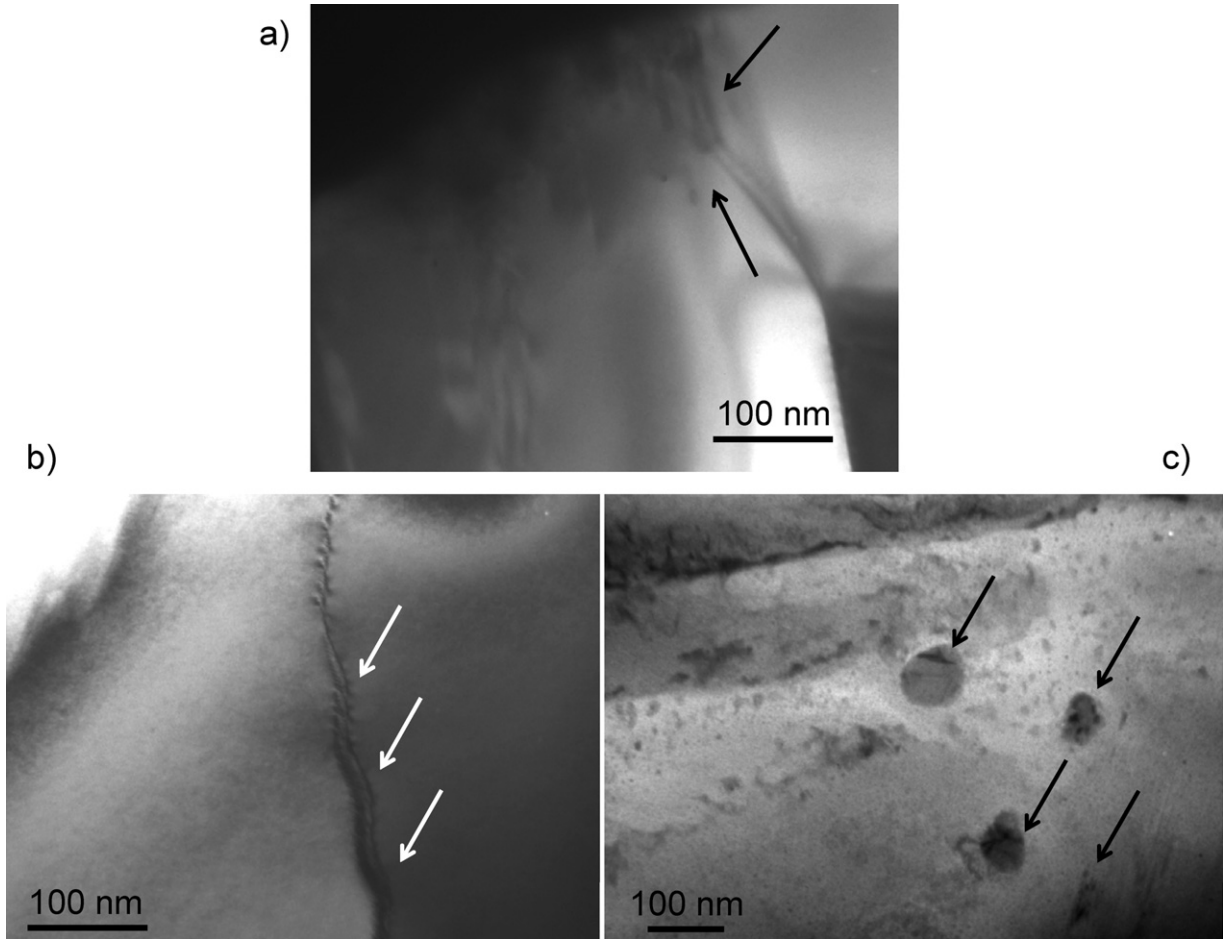

Fig. 9. TEM micrographs showing details of the joint microstructure. (a) Crystal growth at the edge of the reaction layer with the inner part of the joint, (b) dislocations due to plastic deformation generated during brazing, and (c) precipitates corresponding to the Ti rich areas observed by SEM.

metal, and by Ito et al. [30] in brazing Si_3N_4 turbocharger rotors to steel shafts using Ag–Cu–Ni–Ti braze alloys.

Fig. 9 includes TEM higher magnification micrographs in which evidence of the early stages of the titanium nitride and/or titanium silicide formation can be found, the crystal growth being perpendicular to the joint interface (Fig. 9a, arrowed). After an initial thickness of the reaction layer is formed, the process must be controlled by Ti diffusion through this reaction layer. The inner part of the joint (Cu-ABA) shows the presence of dislocations, indicating plastic deformation generated during brazing (Fig. 9b, arrowed), which is in agreement with the EBSD observations. Precipitates are also observed corresponding to the Ti-rich areas detected by EDS (Fig. 9c, arrowed). Because of its relatively low yield strength (278 MPa) and high ductility (42% elongation), plastic deformation of Cu-ABA facilitated accommodation of residual stresses that arise from large temperature excursions ($\Delta T \sim 1273$ K) during brazing and a wide range of coefficients of thermal expansion (CTE) of the phases in the joint. The CTE values of the different phases are [31]: Si_3N_4 ($\alpha = 3.2 \times 10^{-6}$/K), TiN ($\alpha = 9.35 \times 10^{-6}$/K), Ti_5Si_3 ($\alpha = 11 \times 10^{-6}$/K), AlN ($\alpha_c = 5.27 \times 10^{-6}$/K, $\alpha_a = 4.15 \times 10^{-6}$/K) and Cu-ABA ($19.5 \times 10^{-6}$/K). The spatial ordering of the phases in the reaction layer may not correspond to a systematic gradation of CTE from low to high; as a result, complex multi-dimensional residual stresses may be introduced that could cause joint cracking unless these stresses are accommodated by plastic deformation of the braze interlayer.

Several different reactions between Ti or Al (from braze) and silicon nitride are possible, some of which are listed in Fig. 10 together with the corresponding Gibb's free energy change as a function of the temperature, calculated using the software HSC Chemistry version 4.1 (Outokumpu Ra, Oy, Finland). The calculations assume the activity of Ti to be unity. Fig. 10 shows the thermodynamic feasibility of formation of titanium nitride and titanium silicides in joint. The presence of Si and N in the reaction layer indicated that Si and N had diffused in the reaction layer, and probably formed nitrides and silicides as bridging phases that promoted the bonding. The formation of Ti_5Si_3 and AlN was proposed previously in Si_3N_4 joined using Cu-ABA, discarding $TiSi_2$ formation based on the thermodynamic analysis and microstructural observations [32]. It has also been reported [33] that TiN nano-particles form adjacent to the ceramic, and the structure of the Si_3N_4/TiN interface is wavy on an atomic scale, which provides anchoring points for strong bonding. The present work proves the formation of TiN by electron diffraction, and strongly supports the

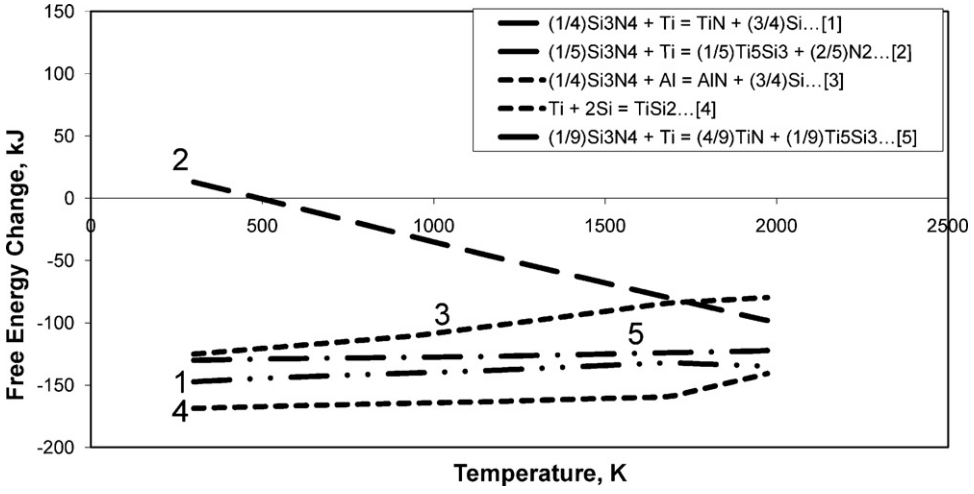

Fig. 10. Gibbs free energy change as a function of temperature for the reaction of Si_3N_4 with Ti and Al from Cu-ABA.

presence of Ti_5Si_3 based on the EDS compositional profiles and maps.

4. Conclusions

Vacuum brazing of Kyocera Si_3N_4 (SN-281) using a ductile Cu–Al–Si–Ti active braze led to sound joints at both 5 min and 30 min brazing times. The morphological homogeneity of the interfacial layers increased with increasing brazing time, and led to a featureless reaction zone in 30 min brazing time due possibly to coarsening and coalescence of the product phase crystals. A Ti-rich reaction layer (∼1.0–2.0 μm thick) developed at the interface, due possibly to the formation of nitrides and/or silicides as bridging phases that promoted the bonding. The joints were crack-free, highly textured, and showed features (e.g., deformation bands) associated with plastic deformation, indicating accommodation of strain associated with CTE mismatch. The orientation of Cu grains in the joint is uniform along the joint plane; however, there is rotation of the grains across the joint, perpendicular to the joint plane. The formation of TiN is detected by electron diffraction, and the presence of Ti_5Si_3 strongly supported by the EDS compositional profiles and maps.

Acknowledgements

Rajiv Asthana and Julian Martinez-Fernandez acknowledge the support received from the NASA Glenn Research Center. Technical assistance received from F. M. Varela-Feria (CITIUS, University of Seville) in SEM and TEM observations is also thankfully acknowledged.

References

[1] K. Suganuma, Y. Miyamoto, M. Koizumi, Joining of Ceramics and Metals, Ann. Rev. Mater. Sci. 18 (1988) 47–73.
[2] S. Peteves, G. Ceccone, M. Paulasto, V. Stamos, P.P. Yvon, Joining silicon nitride to itself and to metals, J. Met. (1996) 48–53.
[3] R.E. Loehman, A.P. Tomsia, J.A. Pask, S.M. Johnson, Bonding mechanisms in silicon nitride brazing, J. Am. Ceram. Soc. 73 (1990) 552–558.
[4] A.P. Tomsia, J.A. Pask, R.A. Loehman, Joining nitride ceramics, Ceram. Eng. Sci. Proc. 10 (1989) 1631–1654.
[5] M. Gopal, M. Sixta, L. De Jonghe, G. Thomas, Seamless joining of silicon nitride ceramics, J. Am. Ceram. Soc. 84 (2011) 708–712.
[6] A.M. Hadian, R.A.L. Drew, Strength and microstructure of silicon nitride ceramics brazed with Ni–Cr–Si alloys, J. Am. Ceram. Soc. 79 (1996) 659–665.
[7] M. Paulasto, G. Ceccone, S.D. Peteves, Joining of silicon nitride with V-active filler metals, in: N. Eustathopoulos, N. Sobczak (Eds.), Proc. Int. Conf. on High-Temperature Capillarity, 29 June–2 July 1997, Cracow, Poland, Foundry Research Institute, Krakow, Poland, 1997 , pp. 290–298.
[8] V.S. Zhuravlev, A.A. Prokopenko, B.D. Kostyuk, I.I. Gab, Y.V. Naidich, Joining of Si3N4 with Ti-active Cu–Ga and Cu–Sn filler alloys, in: N. Eustathopoulos, N. Sobczak (Eds.), Proc. Int. Conf. High-Temperature Capillarity, 29 June–2 July 1997, Cracow, Poland, Foundry Res Institute, Krakow, Poland, 1997, pp. 299–305.
[9] J. Zhang, Y.L. Guo, M. Naka, Y. Zhou, Microstructure and reaction phases in Si_3N_4/Si_3N_4 joints brazed with a Cu–Pd–Ti filler alloy, Ceram. Int. 34 (2008) 1159–1164.
[10] M. Brochu, M.D. Pugh, R.A.L. Drew, Joining silicon nitride ceramic using a composite powder as active brazing alloy, Mater. Sci. Eng. A374 (2004) 34–42.
[11] E. Bader, L. Zoltai, M. Hordler, P. Arato, R.F. Singer, G. Kaptay, Wettability of silicon nitride based ceramics by liquid metals, Trans. JWRI (Japan) 30 (2001) 137–142.
[12] V. Zhuravlev, A. Prokopenko, A. Koval, Wetting of Si_3N_4 by ternary Ti-containing alloys, Trans. JWRI (Japan) 30 (2001) 131–136.
[13] J.-P. Jacquemin, D. Juve, D. Treheux, P. Miranzo, M.I. Osendi, Joining of Si_3N_4 using Al and Ni interlayers, in: A. Bellosi, T. Kosmac, A.P. Tomsia (Eds.), Interfacial Science in Ceramic Joining, Kluwer Academic Publ, Boston, 1998, pp. 135–142.
[14] P. Svec, V. Pulc, E. Gondare, Joining of silicon nitride ceramics to Ti alloy with an interlayer, in: A. Bellosi, T. Kosmac, A.P. Tomsia (Eds.), Interfacial Science in Ceramic Joining, Kluwer Academic Publ, Boston, 1998, pp. 341–348.
[15] G. Blugan, J. Janczak-Rusch, J. Kuebler, Properties and fractography of Si_3N_4/TiN ceramic joined to steel with active single layer and double layer braze filler alloys, Acta Mater. 52 (2004) 4579–4588.
[16] G. Liu, G. Zou, A. Wu, D. Zhang, Improvement of the Si_3N_4 brazed joints with intemetallics, Mater. Sci. Eng. A415 (2006) 213–218.
[17] M. Singh, T.P. Shpargel, R. Asthana, Brazing of yttria-stabilized zirconia (YSZ) to stainless steel using Cu, Ag, and Ti-based brazes, J. Mater. Sci. 43 (2008) 23–32.
[18] M.R. Freedman, Evaluation of Silicon Nitride for Brayton Turbine Wheel Application. NASA/TM-2008-214803, Glenn Research Center, Cleveland, OH, 2008.

[19] C.S. Frazer, E.C. Dickey, A. Sayir, Crystallographic texture and orientation variants in Al_2O_3–$Y_3Al_5O_{12}$ directionally solidified eutectic crystals, J. Crystal Growth 233 (2001) 187–195.
[20] D.G. Coates, Kikuchi-like reflection patterns obtained with scanning electron microscope, Phil. Mag. 16 (1967) 1179–1184.
[21] D.J. Dingley, The development of automated diffraction in scanning and transmission microscopy, in: A.J. Schwartz, M. Kumar, B.L. Adams (Eds.), Electron Backscatter Diffraction in Materials Science, Plenum, New York, 2000.
[22] U.F. Kocks, C.E. Tome, H.R. Wenk, Texture and Anisotropy, Cambridge University Press, Cambridge, 1998.
[23] V. Randle, O. Engler, Introduction to Texture Analysis, CRC Press, New York, 2000.
[24] J.A. Venables, R. Binjaya, Accurate micro-crystallography using electron backscattering patterns, Phil. Mag. 35 (1977) 1317–1332.
[25] S.I. Wright, B.L. Adams, Automated lattice orientation determination from electron backscatter kikuchi diffraction patterns, Texture Microstruct. 14 (1991) 273–278.
[26] S.I. Wright, B.L. Adams, Automatic-analysis of electron backscatter diffraction patterns, Metall. Mater. Trans. A 23 (1992) 759–767.
[27] Pearson's Handbook of Crystallographic Data for Intermetallic Phases, 2nd ed., ASM International, Materials Park, OH, 1991.
[28] H.A. Wriedt, The Al–N system, Bull. Alloy Phase Diagrams 7 (1986) 329–333.
[29] M. Naka, T. Tanaka, I. Okamoto, Joining of silicon nitride to metals or alloys using amorphous Cu–Ti filler metal, Trans. JWRI (Japan) 14 (1985) 285–291.
[30] M. Ito, N. Ishida, N. Kato, Development of brazing technology for ceramic turbocharger rotors, in: Proceedings of Automotive Ceramics – Recent Developments, International Congress and Exposition, Detroit, MI, Feb 29–Mar 04 1988. SAE Technical Paper Series 880704, P207, Society of Automotive Engineers, Warrendale, PA, 1988.
[31] H.O. Pierson, Handbook of Refractory Carbides and Nitrides – Properties, Characteristics, Processing and Applications, Noyes Publications, Westwood, NJ, 1996.
[32] M. Singh, R. Asthana, F.M. Varela, J. Martinez Fernandez, Microstructural and mechanical evaluation of a Cu-base active braze alloy to join silicon nitride ceramics, J. Eur. Ceram. Soc. 31 (2011) 1309–1316.
[33] Iwamoto, S. Tanaka, Interface nanostructure of brazed silicon nitride, J. Am. Ceram. Soc. 81 (1998) 363–368.